Inorganic Chemistry

Article

pubs.acs.org/IC

Comprehensive Vibrational Spectroscopic Investigation of *trans,trans,trans*-[Pt(N$_3$)$_2$(OH)$_2$(py)$_2$], a Pt(IV) Diazido Anticancer Prodrug Candidate

Robbin R. Vernooij,[†,‡,§] Tanmaya Joshi,[†] Evyenia Shaili,[§] Manja Kubeil,[†] Dominique R. T. Appadoo,[∥] Ekaterina I. Izgorodina,[†] Bim Graham,[¶] Peter J. Sadler,[§] Bayden R. Wood,*[,†,‡] and Leone Spiccia*[,†]

[†]School of Chemistry and [‡]Centre for Biospectroscopy, Monash University, Melbourne, 3800 VIC, Australia

[§]Department of Chemistry, University of Warwick, Gibbet Hill Road, Coventry CV4 7AL, U.K.

[∥]Australian Synchrotron, 800 Blackburn Road, Clayton, 3168 VIC, Australia

[¶]Monash Institute of Pharmaceutical Sciences, Monash University, Melbourne, 3052 VIC, Australia

Supporting Information

ABSTRACT: We report a detailed study of a promising photoactivatable metal-based anticancer prodrug candidate, *trans,trans,trans*-[Pt(N$_3$)$_2$(OH)$_2$(py)$_2$] (**C1**; py = pyridine), using vibrational spectroscopic techniques. Attenuated total reflection Fourier transform infrared (ATR-FTIR), Raman, and synchrotron radiation far-IR (SR-FIR) spectroscopies were applied to obtain highly resolved ligand and Pt-ligand vibrations for **C1** and its precursors (*trans*-[Pt(N$_3$)$_2$(py)$_2$] (**C2**) and *trans*-[PtCl$_2$(py)$_2$] (**C3**)). Distinct IR- and Raman-active vibrational modes were assigned with the aid of density functional theory calculations, and trends in the frequency shifts as a function of changing Pt coordination environment were determined and detailed for the first time. The data provide the ligand and Pt-ligand (azide, hydroxide, pyridine) vibrational signatures for **C1** in the mid- and far-IR region, which will provide a basis for the better understanding of the interaction of **C1** with biomolecules.

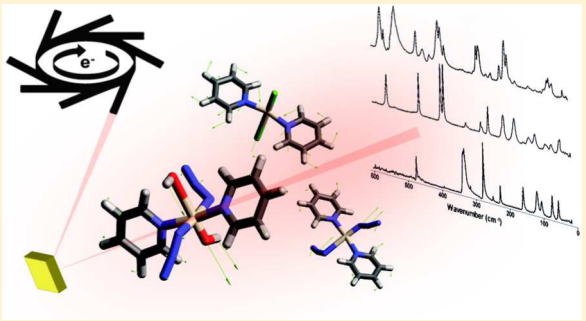

INTRODUCTION

Cancer chemotherapy is landmarked by the indisputable clinical success of cisplatin,[1−3] with ca. 50% of all the cancer patients receiving a platinum compound.[4] Disappointingly, however, platinum therapy suffers from several drawbacks, which include acquired resistance, limited spectrum of activity, and toxic side effects.[5−7] Consequently, constant efforts are being made to develop new generations of metallo-pharmaceuticals that address these shortcomings, including the design of less toxic Pt(IV) prodrugs, which are activated in cancer cells either by (bio)chemical or photoinduced reduction.[8−19]

Localized treatment of cancer by light builds upon the clinically established photodynamic therapy (PDT), which produces highly reactive singlet oxygen species ($^1O_2$) by energy transfer from light to photosensitizers and subsequently to ground-state triplet oxygen ($^3O_2$). However, PDT relies on the presence of oxygen at the targeted treatment site, which is a major drawback, as many malignant and most aggressive tumors are hypoxic by nature.[20] By contrast, local activation of metal-based prodrugs by light, also referred to as inorganic photoactivated chemotherapy (PACT), offers the possibility of oxygen-independent treatment, where reactive (metal-based) species are formed upon irradiation.[21−28]

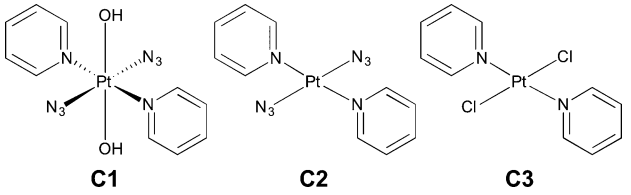

Figure 1. Structures of platinum complexes studied in this work: *trans,trans,trans*-[Pt(N$_3$)$_2$(OH)$_2$(py)$_2$] (**C1**), *trans*-[Pt(N$_3$)$_2$(py)$_2$] (**C2**), and *trans*-[PtCl$_2$(py)$_2$] (**C3**).

The *trans,trans,trans*-[Pt(N$_3$)$_2$(OH)$_2$(py)$_2$] (**C1**; Figure 1) species is one such promising inert and nontoxic platinum(IV) diazido anticancer prodrug candidate for PACT, which can be locally activated in cancer cells under UV-A and visible light irradiation while being stable in the dark under biological conditions.[10,14,29−31] Upon photoactivation, **C1** undergoes changes in the metal coordination environment, giving rise to Pt(II), nitrene, and radical photoproducts, as well as cleaved ligands, which act in concert to elicit the observed multitargeted biological activity;[10] irradiation of **C1** results in stalling of RNA polymerase II and an ∼16-fold increase in DNA "platination" compared to cisplatin.[32]

Received: February 25, 2016
Published: June 3, 2016

DOI: 10.1021/acs.inorgchem.6b00476
Inorg. Chem. 2016, 55, 5983−5992

The exact mechanism of action of **C1**, however, is not completely understood.

Vibrational spectroscopic studies of biological samples and biomolecule−drug interactions constitute a rapidly expanding research area because of the increase in throughput, improvements in spatial resolution, and availability of methodology to process large data sets, while at the same time being label-free and nondestructive.[33] Of particular interest to us is the fact that it allows changes in the metal coordination environment to be monitored in the mid- and far-IR spectral regions. This can be extremely useful for studying metal-containing drugs, particularly those containing functionalities with unique vibrational bands (e.g., azido, nitrosyl, cyano, and carbonyl groups).

Given that previous efforts to elucidate the mechanism of actions of **C1** have shown that the activity is indeed associated with changes in metal coordination environment, vibrational spectroscopy becomes a useful tool to investigate further its multitargeted biological activity.[34−40] Previous mechanistic studies have revealed that wavelength-dependent photodecomposition of these Pt(IV) complexes gives rise to Pt-nitrene intermediates, singlet oxygen, free azide, and azidyl radicals capable of oxidizing a biomolecular target, 5′-guanosine monophosphate.[10,13,14] With its ability to provide functional group analysis, vibrational spectroscopy can serve to monitor the complex processes occurring upon irradiation and to assess binding sites of such metal-based (pro)drug candidates following activation.

Herein, vibrational spectroscopy studies are presented, which have allowed a detailed assignment of ligand and metal−ligand vibrational modes for **C1**, the diazido Pt(IV) anticancer prodrug candidate, and two of its synthetic Pt(II) precursors, *trans*-$[Pt(N_3)_2(py)_2]$ (**C2**; Figure 1) and *trans*-$[PtCl_2(py)_2]$ (**C3**; Figure 1). Three vibrational spectroscopic techniques, specifically, ATR-FTIR, Raman, and synchrotron radiation far-IR spectroscopy (SR-FIR) were used to assign all the vibrations, assisted through vibrational mode predictions obtained from the density functional theory (DFT) calculations on **C1**−**C3**. Although **C1** has been subjected to several biological studies, no vibrational spectroscopic investigations have been conducted to date. The measured frequency data provide the infrared and Raman-active vibrational fingerprints for **C1**, which is an essential first step toward elucidating the complex mechanism of action and intermolecular interactions of **C1** and other such Pt(IV) (pro)drug candidates using vibrational spectroscopic techniques.

RESULTS AND DISCUSSION

Measurements were performed as described in the Experimental Section. It is important to note that the use of aqueous media (buffers and/or cell media) is preferred when carrying out in vitro studies aimed at understanding the mechanism of action such drug candidates. Thus, it is equally important to assign thoroughly the vibrational fingerprints of **C1** after exposure to such media. For this purpose, dissolution of **C1** in water followed by evaporation (hereafter referred to as **C1**′) was performed prior to measuring ATR-FTIR and Raman spectra and compared to the spectra of crystalline **C1**. To confirm comparison is possible between spectra obtained by the diamond and silicon ATR accessories, 9 μL (diamond) and 3 μL (Si) solutions of **C1** (2 mM) were deposited on the ATR accessories, and no discernible differences between the spectra were observed (Figure S13). Only the silicon ATR results of **C1**′ are reported throughout this manuscript.

Ground-state lowest energy (S_0) geometries, computed by theoretical calculations as described in the Experimental Section, were compared to the previously reported crystal structures, and closest matches from both PBE (Figure 2) and M06-2X were used to fit the experimental vibrational results.[10,41,42] Two S_0 geometries of lowest energy (Figure 2, **C2−1** and **C2−2**, ΔE = 3.1 kJ/mol) were used for **C2** to account for the two conformations observed in its crystal structure.[41]

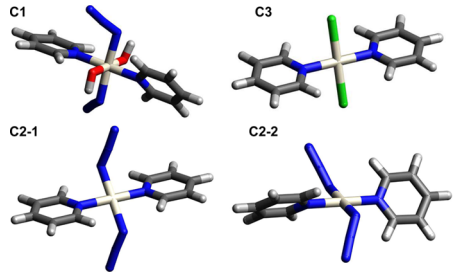

Figure 2. Lowest energy geometries optimized by DFT with PBE for **C1**, **C3**, **C2−1**, and **C2−2**. Calculations were performed with cc-pVDZ for C, H, N, and O and with cc-pVDZ-PP[44] with ECP for Pt using the CPCM with water as solvent.

Selected bond distances and angles of **C1**, **C2**, and **C3** and the computed results are shown in Tables S1−3 of the Supporting Information. The full assignments for the individual complexes (Tables S4−S6), Cartesian coordinates of all S_0 geometries, calculated IR frequencies, including assignments and a description of planes (Figure S1) used for vibrational assignment can also be found in the Supporting Information. The vibrational modes of pyridine coordinated to platinum are derived from Wilson's notation for benzene and are shown in Figure S2 to avoid discrepancies in nomenclature.[43] Selected ATR-FTIR, Raman, SR-FIR, and unscaled theoretical PBE vibrational bands of **C1**, **C2**, and **C3** are shown in Table 1 (see Supporting Information for comments on scaling of vibrational frequencies). The SR-FIR spectra of **C1**, **C2**, and **C3** at room temperature versus 77 K are depicted in Figures S9−S11.

The discussion of the vibrational data for **C1**−**C3** below is subdivided according to the individual types of ligand vibrations (pyridine, hydroxido, and azido) and metal−ligand vibrations, with some suggestions as to how these vibrations could be monitored to analyze the photodecomposition of **C1**.

Pyridine Vibrations. Many fundamental vibrational spectroscopic studies of pyridine and derivatives thereof have been reported to date, including for pyridine bound to various surfaces.[45−53] The pyridine vibrations were very well-defined in the spectra of **C1**, **C2**, and **C3** and could be readily assigned (see Table S4−6). These are in agreement with previously reported results, with the vibrational frequencies shifted relative to free pyridine in the manner expected.[53−55] Selected CH stretching vibrations, ring deformations, and CH bending vibrations of pyridine measured by ATR-FTIR are shown in Figure 3. The spectra clearly demonstrate that a change in the neighboring ligands, molecular geometry, or crystal packing does not have a major influence on the intensities and wavenumber values of the pyridine vibrations, which is in line with the calculated results.

The medium-to-strong IR and weak Raman bands at 1611 cm^{-1} (IR and Raman) for **C1**, 1610 cm^{-1} (IR)/1611 (Raman) **C2** and 1608 cm^{-1} (IR)/1609 cm^{-1} (Raman) for **C3** are assigned to the IR- and Raman-active ring stretching mode of pyridine; δ(py) {A_1, 8a}. While this band has been reported as weak in the Raman spectrum of free pyridine, the *trans* positioning of pyridines allows for in-phase bending, which symmetrically

DOI: 10.1021/acs.inorgchem.6b00476
Inorg. Chem. 2016, 55, 5983−5992

Table 1. Selected ATR-FTIR, Raman, SR-FIR, and Unscaled Theoretical Vibrational Bands of C1, C2, C3 (Solid), and C1′ (Dissolution of C1 in Water Followed by Evaporation Prior to Measurements)

no.	vibrations[a,b]	*trans,trans,trans*-$[Pt(N_3)_2(OH)_2(py)_2]$ **C1/C1′** (cm^{-1})[c]										*trans*-$[Pt(N_3)_2(py)_2]$ **C2** (cm^{-1})[c]					*trans*-$[PtCl_2(py)_2]$ **C3** (cm^{-1})[c]				
		IR[d]		IR′		Raman[e]		Raman′[e]		calcd[f]		IR[d]		Raman[e]		calcd[f]	IR[d]		Raman[e]		calcd[f]
1	υ(OH)	3566	s	3551	s	3571	w	3560	w	3610											
2	$\upsilon(CH_{py})$	3113–3009	m - w	3127–3014	m - w	3084	m	3094–3057	m–w	3185–3106		3116–3007	m - w	3087, 3072	m	3170–3138	3113–3005	m - w	3089–3069	m- w	3170–3139
3	$\upsilon_{asym}(N_3)$							2068	s												
4		2051	vs	2048	s, sh	2053	s	2053	s			2066	vs	2057	w, br						
5		2035	s, sh	2033	vs	2040	w, sh			2117		2039	s, sh			2114					
6		2017	vs	2003	m, sh	2028	m			2101		2002	s, sh			2098					
7		1984	m, sh	1979	m, sh	2018	m														
8		1965	m, sh									1958	m, sh								
9		1942	w, sh	1947	m, sh							1942	m, sh								
10	δ(py) {A_1, 8a}	1611	m	1612	m	1611	m	1612	m	1615		1610	m	1611	m	1611	1608	s	1609	m	1612
11	δ(py) {B_2, 19b}	1458	s	1460	s					1442		1455	m			1437	1451	vs			1437
12	$\upsilon_{sym}(N_3)$	1292	s	1278	m, sh	1291	w	1290	w	1299				1325	m	1300					
13		1271	s	1271	s	1282	w	1281	w	1290		1294	m	1298	w	1291					
14	δ(py) {B_2, 18b}	1074	m	1076	m	1078	w			1071		1077	m	1080	w	1067	1072	s	1079	m	1069
15	δ(py) {A_1, 12}					1027	s	1028	s	1015				1025	vs	1015			1024	vs	1032
16	γ(py) {B_1, 4}	777	s	772	s					757		772	m			749	771	vs			751
17	γ(py) {B_1, 11}, $\delta(N_3)$[g]	697	s	696	s, sh					693, 676							691	vs			676
18		684	s, sh	686	s	684	s	680	s	665, 667		696	m			675, 668					
19	δ(py) {A_1, 6a}	660	w	656	m	662	m, sh	664	m, sh	640		670	w, sh	662	w	637	660	w, sh	664	w	639
20	δ(py) {B_2, 6b}	645	m			647	w, sh	649	m, sh	633		650	w	647	w	634			649	w	634
21	$\gamma(N_3)$	584	s			582	s	584	m, sh	561		568	s			558					
22		573	m					571[h]	s	560											
23	υ_{asym}(HO–Pt–OH)	561	w																		
24		553	w, sh																		
25		545	s, sh																		
26		541	s							529											
27	υ_{sym}(HO–Pt–OH)					540	s			524											
28	γ(py) {B_1, 16b}	478	m							467		472	s			468	484	m			478
29	$\upsilon_{asym}(N_3–Pt–N_3)$	417	m, sh																		
30		413	s							389		408	s			384					
31		407	s									400	s			382					
32		395	m																		
33	$\upsilon_{sym}(N_3–Pt–N_3)$					415	vs	414	vs	389				406	m	391					
34	υ_{asym}(Cl–Pt–Cl)																346	s			
35																	342	s			318
36																	339	m, sh			
37	scr(HO–Pt–OH), scr $(N_3–Pt–N_3)$	301	m							309											
38	υ_{sym}(Cl–Pt–Cl)																324	w	326	m	302
39	υ_{asym}(Cl–Pt–Cl)																286	s			282
40	υ_{asym}(py–Pt–py)[i]	258	w							247		269	s			248	258	w			241

DOI: 10.1021/acs.inorgchem.6b00476
Inorg. Chem. 2016, 55, 5983–5992

Table 1. continued

no.	vibrations[a,b]	*trans,trans,trans*-$[Pt(N_3)_2(OH)_2(py)_2]$ **C1/C1′** (cm^{-1})[c]							*trans*-$[Pt(N_3)_2(py)_2]$ **C2** (cm^{-1})[c]				*trans*-$[PtCl_2(py)_2]$ **C3** (cm^{-1})[c]			
		IR[d]		IR′	Raman[e]		Raman′[e]	calcd[f]	IR[d]		Raman[e]		calcd[f]	IR[d]		Raman[e]		calcd[f]
41	υ_{sym}(py−Pt−py)	217	s		217	s	214	m, sh	217		216	m, sh	214			216	w	214
42	scr(Cl−Pt−Cl)													169	m			150
43	δ(Pt−N_3) out-of-phase	140	w, sh		143	s	132	s	127	149	w	139	s	131				
44	δ(Pt−N_3) in-phase	125	w		120	m, sh	122	m, sh	105	131	m	123	vs	129				
45	wag(Cl−Pt−Cl)														126	m		118
46	Lattice vibrations[j]	92	m					69										
47		87	m					59	83	w			68	83	m		49	
48		81	m, sh															
49		77	m					50										
50		46	m					43	59	m, sh			49	64	m		36	
51									56	m			47					

[a]Only the predominant and/or discussed vibrations are displayed; see Supporting Information for full descriptions. [b]Notations used: υ = stretch, δ = in-plane angle bending, γ = out-of-plane angle bending, wag = wagging, scr = scissoring, rot = rotation, sym = symmetric, and asym = asymmetric. Out-of-phase and in-phase notations refer to the phase between dissimilar vibrations or analogous vibrations when more than one of the same moieties exists. The descriptions of pyridine modes are given in Wilson's notations; see Supporting Information Figure S2.[43] [c]Peak intensities: vs = very strong, s = strong, m = medium, w = weak, br = broad, and sh = shoulder. [d]4000−650 cm^{-1} = corrected ATR-FTIR and 650−0 cm^{-1} = SR-FIR at 77 K. [e]633 nm excitation. [f]Unscaled PBE vibrations; see Supporting Information for M06-2X results. [g]$\delta(N_3)$ is overlapped by γ(py) {B_1, 11} for **C1**. [h]Tentative assignment; this particular vibration could also be originating from υ_{sym}(HO−Pt−OH) for **C1′**. [i]υ_{asym}(py−Pt−py) is a combination band with scr(N_3−Pt−N_3) + rot(Pt−OH) for **C1** and scr(N_3−Pt−N_3) for **C2**. [j]See text and Supporting Information for discussion of lattice vibrations.

elongates the Pt−py distances, increasing the Raman cross-section of this mode.[53,55]

The position of the fundamental pyridine deformation vibration, δ(py) {A_1, 6a}, has previously been reported to have a nearly linear relationship with the change in the force constant of the ligand−metal bond, suggesting that the strength of the interaction of pyridine and a metal atom (surface) can be gauged by frequency shifts of this mode.[51] In this case, differences were observed in the δ(py) vibrations for Pt(IV) and Pt(II), **C1**/**C1′** (660/656 cm^{-1}), and **C2**/**C3** (670/660 cm^{-1}), by ATR-FTIR only. The Raman spectra did not reveal such a change (662 cm^{-1} **C1**, 662 cm^{-1} **C2**, and 664 cm^{-1} **C3**), and the calculated values did not predict a significant change (640 cm^{-1} **C1**, 638 cm^{-1} **C2**, and 639 cm^{-1} **C3**).

The SR-FIR spectra show medium-to-strong intensity bands for the out-of-plane ring deformation γ(py) {B_1, 16b} of pyridine for **C1**, **C2**, and **C3**. Substitution of the chlorido ligands with azido ligands resulted in a notable shift in band position from 484 cm^{-1} (**C3**) to 472 cm^{-1} (**C2**), which shifts to 478 cm^{-1} in **C1**, as **C2** is subsequently oxidized and two additional hydroxido ligands are introduced into the Pt(IV) coordination sphere.

In the SR-FIR spectrum at 77 K (Figure 6), two well-defined lattice vibrations of medium intensity are observed for **C3** at 83 and 64 cm^{-1} and three broader bands of medium-to-weak intensity for **C2** at 83, 59 (sh), and 56 cm^{-1}. In contrast, five well-defined lattice vibrations are observed for **C1** at 92, 87, 81, 77, and 46 cm^{-1}. Such an increase in the number of lattice modes is to be expected given the increase in degrees of freedom when going from square-planar to octahedral geometry. Note that even though several rotational and translational motions of pyridine in the matching wavenumber range were predicted by DFT calculations for **C1**, **C2**, and **C3** (Supporting Information), we refrain from assigning them to the experimental data unlike the other vibrations of higher wavenumber values. Calculated translational modes are expected to be close to zero (within 10 cm^{-1}) due to the nature of frequency calculations, whereas rotational modes need to be treated using higher-level approximations beyond the harmonic oscillator for meaningful results, which was outside the scope of this work.

Hydroxido Vibrations. ATR-FTIR and Raman spectra reveal single hydroxido stretching vibrations, υ(OH), for **C1** crystals at 3566 and 3571 cm^{-1}, respectively (Figures S6 and S8). These bands were matched by the calculated results and are in accordance with other platinum−hydroxido stretching vibrations.[56−60] Upon dissolution of **C1** in water, followed by evaporation, this vibration is reduced by 15 cm^{-1} by IR and by 11 cm^{-1} by Raman. The presence of intermolecular hydrogen bonding observed in the crystal structure between hydroxido ligands of neighboring complexes is also evident by ATR-FTIR spectroscopy, as seen by the broad medium band peaking at ∼3200 cm^{-1}.[10]

Azido Vibrations. Linear triatomic molecules ($D_{\infty h}$), such as azide, have four theoretical vibrational modes; asymmetric and symmetric stretching ($\upsilon_{asym}(N_3)$, $\upsilon_{sym}(N_3)$) and the doubly degenerate bending vibrations ($\delta(N_3)$, $\gamma(N_3)$). Multiple bands for the asymmetric azido stretch, $\upsilon_{asym}(N_3)$, are observed by ATR-FTIR and Raman spectroscopy for both complex **C1**, **C1′**, and **C2**, which were matched to the calculated vibrations (Table 1). $\upsilon_{asym}(N_3)$ is a symmetry-forbidden Raman transition; however, the out-of-phase asymmetric azido vibration ($\upsilon_{asym}(N_3)$) and crystal packing give rise to the Raman-active asymmetric vibrations. This also applies to the symmetrical azido stretching vibration ($\upsilon_{sym}(N_3)$).

DOI: 10.1021/acs.inorgchem.6b00476
Inorg. Chem. 2016, 55, 5983−5992

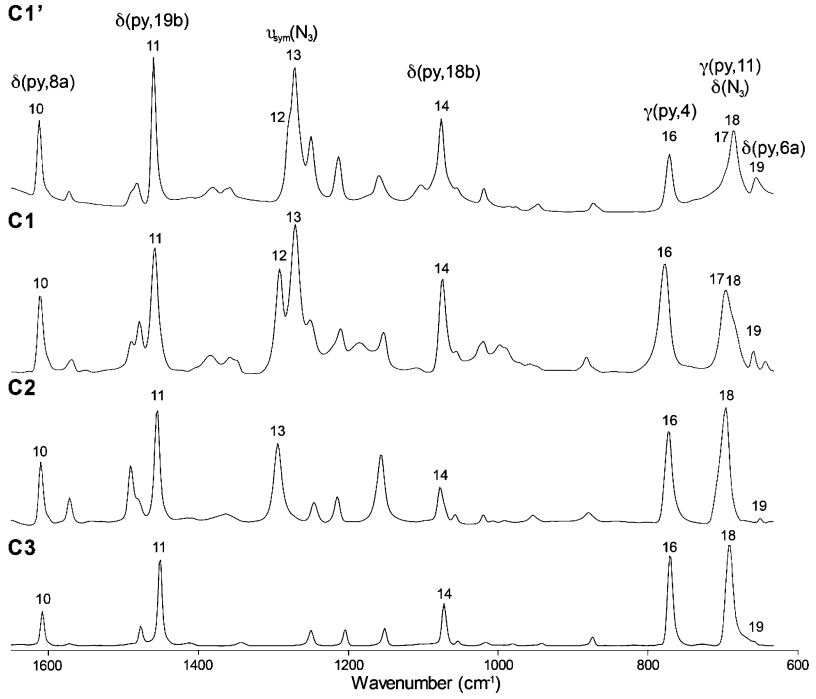

Figure 3. ATR-FTIR spectra of **C1**, **C2**, **C3** (solid) and **C1**′ (dissolution of **C1** in water followed by evaporation prior to measurements).

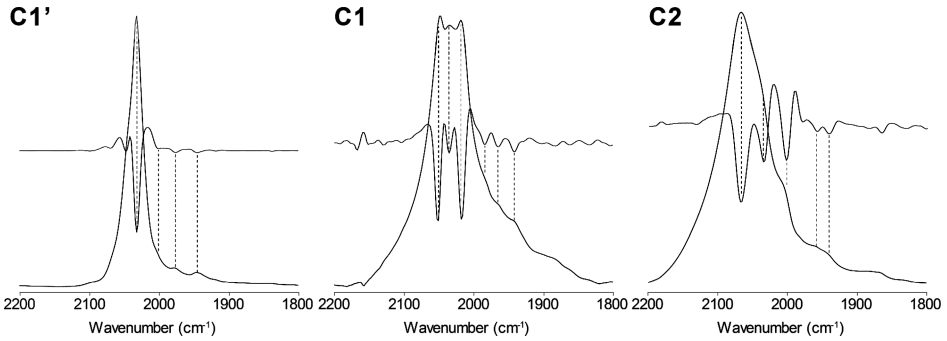

Figure 4. ATR-FTIR spectra overlapped with the second derivative for **C1** (solid), **C2** (solid), and **C1**′ (dissolution of **C1** in water followed by evaporation prior to measurements) highlighting $\upsilon_{asym}(N_3)$ changes going from **C2** to **C1** and the effect of dissolution followed by evaporation of **C1** prior to measurement (**C1**′).

Six $\upsilon_{asym}(N_3)$ bands were identified from the second derivative ATR-FTIR spectrum of **C1** and five for **C1**′ and **C2** (Figure 4). Such a splitting of bands is expected due to factor group splitting, different platinum−nitrogen (N_3) and nitrogen−nitrogen (N_3) bond lengths and angles, in-phase and out-of-phase vibrations, intermolecular hydrogen bonding, and longer distance interactions. Platinum and other heavy metal azido compounds with similar splitting of vibrations have been reported.[61,62]

As mentioned above, dissolution of **C1** in water, followed by evaporation prior to measurement (**C1**′) has no significant effect on the pyridine vibrations but does effect the hydroxido vibration. Furthermore, differences in all azido vibrations ($\upsilon_{asym}(N_3)$, $\upsilon_{sym}(N_3)$, $\delta(N_3)$, and $\gamma(N_3)$) are observed between **C1** and **C1**′ in both the ATR-FTIR and Raman spectra (Table 1). Notably, changes in the intermolecular interactions of **C1** are most evident from the shifts in the main $\upsilon_{asym}(N_3)$ vibrations (**C1** to **C1**′; 2051 to 2033 cm^{-1} IR, 2053 cm^{-1} to 2068/2053 cm^{-1} Raman) and the decrease in the number of bands observed (six to five IR, four to two Raman).

Five $\upsilon_{asym}(N_3)$ vibrations were observed by ATR-FTIR for **C2** (Figure 4). However, for **C2** only one weak broad Raman band is observed for $\upsilon_{asym}(N_3)$ at 2057 cm^{-1}, whereas **C1** and **C1**′ have multiple bands of medium intensity as described above. This could be due to the change in geometry going from Pt(IV) to Pt(II), allowing for less dissymmetry and in turn weaker Raman bands.

The symmetric azido vibration, $\upsilon_{sym}(N_3)$, is observed in the ATR-FTIR spectra at 1292/1271 cm^{-1} for **C1** and 1294 cm^{-1} for **C2**, whereas the corresponding Raman bands are at 1291/1282 cm^{-1} (**C1**) and 1325/1298 cm^{-1} (**C2**). The first degenerate bending vibration, $\delta(N_3)$, overlaps with the out-of-plane pyridine bending vibration in the ATR-FTIR; γ(py) {B_1, 11}, $\delta(N_3)$ for **C1** (697/684 cm^{-1}) and **C2** (696 cm^{-1}). The second azido bending vibration, $\gamma(N_3)$, is observed as one strong band at 568 cm^{-1} in the SR-FIR spectrum of **C2**. Notably, the asymmetry of **C1** splits this band into two peaks at 584 and 573 cm^{-1}.

At this stage, differences in the splitting of the azido vibrations in the ATR-FTIR and Raman spectra arising from crystal packing effects cannot be ruled out. **C1** crystallizes in an orthorhombic system, *Pbca*, and contains eight formula units per unit cell (Z = 8), allowing for factor group splitting. Furthermore,

DOI: 10.1021/acs.inorgchem.6b00476
Inorg. Chem. 2016, 55, 5983−5992

one azido ligand has a longer contact (2.630 Å) with an oxygen of a neighboring complex.[10] The crystal structure of **C2** (monoclinic, I121, $Z = 2$) revealed disordered pyridines over approximately two orientations.[41] Additionally, **C1** and **C2** contain two *trans*-azido ligands, which allow for in-phase and out-of-phase vibrations (see model of **C1** in Figure 5).

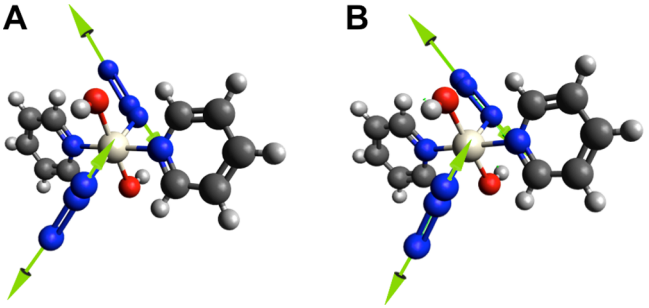

Figure 5. Visualization of the $\upsilon_{asym}(N_3)$ in-phase (A) and $\upsilon_{asym}(N_3)$ out-of-phase (B) in a model of **C1**. M06-2X/cc-pVDZ for C, H, N, and O and cc-pVDZ-PP[44] with ECP for Pt using the CPCM with water as solvent.

The asymmetry of **C1**, observed in the crystal structure and optimized structures, can give rise to IR active in-phase and out-of-phase $\upsilon_{asym}(N_3)$ vibrations as indicated by the DFT calculations.

Metal–Ligand Vibrations. The SR-FIR spectra of **C1**, **C2**, and **C3** are illustrated in Figure 6. Many of the bands are highly defined due to the increased factor group splitting at 77 K and the use of synchrotron radiation. The theoretical calculations are in good agreement with the measured spectra, and multiple bending vibrations accompany the majority of the bands (see Supporting Information, Tables S4–S6). The main platinum–ligand stretches and bending modes are discussed here. Strong platinum-oxygen (OH) stretching bands are observed for the asymmetric stretching vibration; υ_{asym}(HO–Pt–OH) at 545 and 541 cm^{-1}, with multiple weak shoulders observed in the SR-FIR spectra as well as one strong Raman band at 540 cm^{-1}, corresponding to the symmetric stretching vibration υ_{sym}(HO–Pt–OH). These assignments are in agreement with a recent reinterpretation of the vibrational assignments for *cis,cis,trans*-$[Pt(NH_3)_2Cl_2(OH)_2]$, which reported stretching vibrations for υ_{asym}(HO–Pt–OH) and υ_{sym}(HO–Pt–OH) at 575 and 559 cm^{-1}, respectively.[56,59] The splitting of multiple bands by IR can be explained by the crystal structure of **C1**, which contains eight formula units per unit cell. Furthermore, one hydroxido hydrogen of **C1** is involved in hydrogen bonding to an oxygen (1.989 Å) on a neighboring complex, while the other has a longer contact (2.630 Å) to the azido group of a neighboring complex and its oxygen is involved in hydrogen bonding to a hydrogen of a different neighboring complex.[10] The corresponding bending vibration, scr(HO–Pt–OH), was matched to the 301 cm^{-1} band in the SR-FIR spectrum.

Four bands were identified in the SR-FIR spectrum of **C1** for the platinum–nitrogen (N_3) asymmetric stretch, $\upsilon_{asym}(N_3–Pt–N_3)$ at 417, 413, 407, and 395 cm^{-1}, whereas two bands are observed for **C2** at 408 and 400 cm^{-1}. **C2** is known to crystallize with the pyridines disordered over approximately two orientations;[41] this is well-reflected in the two well-defined bands of equal intensity separated by 8 cm^{-1}. Separation between the respective bands was also present in the theoretically predicted spectra of the two S_0 structures, **C2–1** and **C2–2**. The calculated difference from the M06-2X functional was 12 cm^{-1}, whereas a smaller difference of 2 cm^{-1} was obtained with the PBE functional. As described in the azido vibration section, **C1** crystallizes in an orthorhombic system (*Pbca*, $Z = 8$) and has two different azido orientations relative to the platinum center. It also exhibits intermolecular hydrogen bonding and longer distance interactions, which contribute to this splitting of $\upsilon_{asym}(N_3–Pt–N_3)$.

Earlier IR spectroscopic studies on $[Pt(N_3)_6]^{2-}$ and $[Pt(N_3)_4]^{2-}$ revealed that the $\upsilon(Pt–N_3)$ occur at 410/400 cm^{-1} and 408/394 cm^{-1} respectively, in line with our results.[62,63] A very strong and narrow symmetric platinum–nitrogen (N_3) stretching vibration, $\upsilon_{sym}(N_3–Pt–N_3)$, is observed for **C1** and **C1′** in the Raman spectrum at 415 and 414 cm^{-1} (Figures 7, S6, and S7), while only a medium intensity band at 406 cm^{-1} is observed for **C2**. The increase in intensity going from **C2** to **C1** is most likely related to the oxidation state of platinum and addition of hydroxido ligands. Thus, changes to the geometry/oxidation state of **C1** upon irradiation can potentially be monitored by the $\upsilon_{sym}(N_3–Pt–N_3)$ Raman vibration. However, in the case of **C2**

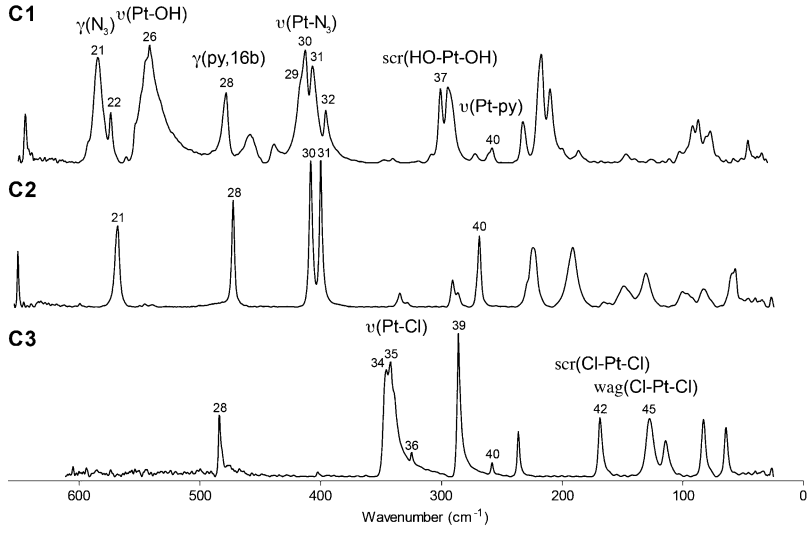

Figure 6. SR-FIR spectra of solid **C1**, **C2**, and **C3** measured at 77 K.

DOI: 10.1021/acs.inorgchem.6b00476
Inorg. Chem. 2016, 55, 5983–5992

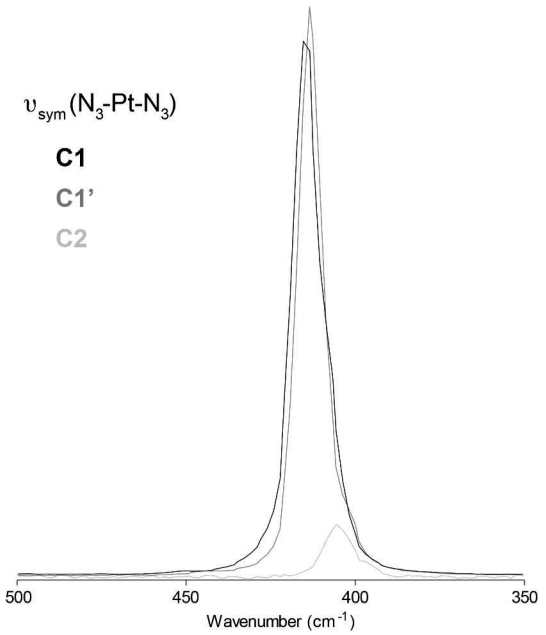

Figure 7. Normalized Raman spectra of **C1** (solid), **C2** (solid), and **C1′** (dissolution of **C1** in water followed by evaporation prior to measurements).

an unusually strong band is located at 269 cm^{-1} in the SR-FIR spectrum, and it is well-separated from other vibrational modes.

An IR-active asymmetric platinum−nitrogen (py) stretch, υ_{asym}(py−Pt−py), is predicted by both M06-2X (243 m) and PBE (248 w) in combination with in-phase scissoring of N_3−Pt−N_3; scr(N_3−Pt−N_3). Furthermore, the diazido Pt(II) complex **C2** adopts an unusual crystal packing, with a twofold axis of symmetry, where the dihedral angle between platinum and azide is −107° (Pt−N−N−N). The azido ligand is bent with an internal NNN angle of 159°, with distances to three pyridine hydrogens in neighboring complexes of 2.401, 2.524, and 2.604 Å, which are in nearly the same plane (Table S2 and Figure S12). This crystal packing would greatly enhance the intensity of a vibration such as υ_{asym}(py−Pt−py) + scr(N_3−Pt−N_3) in-phase (i.e., bending of Pt−N_3 toward the elongating Pt−py) as shown by the experimental values. The Pt(IV) complex **C1** and dichloride Pt(II) complex **C3** do not show such an enhancement in intensity, and their experimental υ_{asym}(py−Pt−py) vibrations were matched by the results of computation. The weak experimental band for **C1** at 258 cm^{-1} corresponds well to a calculated vibration of υ_{asym}(py−Pt−py) + scr(N_3−Pt−N_3) + rot(Pt−OH), whereas the weak sharp peak present in the spectrum of **C3** at 258 cm^{-1} matches the calculated vibration for υ_{asym}(py−Pt−py).

Far-IR spectra of **C3** have been previously reported and correlate well with the SR-FIR spectra.[64−66] Adams et al.[64] observed bands at 343 (vs), 327 (sh), and 283 (vs) cm^{-1} related to Pt−Cl stretches, which match our observed bands at 346/342/339 (s), 324 (w), and 286 (s) cm^{-1}. Some **C3** bands show slight asymmetric line shapes (Figure 6) compared to **C1** and **C2**. This is due to more pronounced anomalous dispersion in **C3** compared to the other compounds, and therefore the true maxima of these bands might be slightly shifted to longer wavenumber values.[67] Assignments were not discussed in detail by Adams et al.;[64] however, the results of computation allowed the assignment of two different asymmetric Pt−Cl stretching vibrations at 346/342/339 cm^{-1} (υ_{asym}(Cl−Pt−Cl), rot(py) {A_2, ωz} in-phase, in-phase) and 286 cm^{-1} (υ_{asym}(Cl−Pt−Cl), rot(py) {A_2, ωz} in-phase, out-of-phase). These asymmetric stretching vibrations are combination bands with in-phase rotation of pyridine (rot(py) {A_2, ωz} in-phase), which occur in-phase and out-of-phase with one another, that is, dipole change in one direction (in-phase) or opposite direction (out-of-phase). The splitting of the υ_{asym}(Cl−Pt−Cl) vibration at ∼346 cm^{-1} is indicative of intermolecular coupling and hydrogen bonding, which is not reflected in the previously reported crystal structure. The 324 cm^{-1} SR-FIR band of **C3** coincides with the Raman band at 326 cm^{-1} and is assigned as the symmetric Pt−Cl vibration; υ_{sym}(Cl−Pt−Cl). The two bending vibrations, scr(Cl−Pt−Cl) and wag(Cl−Pt−Cl), were matched to computed values of 169 and 126 cm^{-1}.

Monitoring the Reactivity of C1. The vibrational spectra described above revealed marker bands in the mid- and far-IR regions, which might be used to monitor the photodecomposition and/or photoinduced biomolecular interactions of the photoactive Pt(IV) diazido complex **C1**. The upper end of the mid-IR region (4000−3000 cm^{-1}) contains signature vibrations for **C1** consisting of the hydroxido stretching vibration, υ(OH), at 3566/3571 cm^{-1} (IR/Raman) and several pyridine stretching vibrations, υ(CH), between 3113 and 3009 cm^{-1}. Strong bands are observed for the asymmetric azido stretch, υ_{asym}(N_3) of **C1** and **C1′** at ∼2051−2017 cm^{-1}, which are separated by at least 200 cm^{-1} from vibrations associated with natural molecules in biological samples.[33] The lower end of the mid-IR region (1600−600 cm^{-1}) mainly consists of pyridine vibrations, all of which were assigned individually, and the symmetric azido stretches at 1271/1282 cm^{-1} (IR/Raman). The Raman and ATR-FTIR analysis of **C1** following dissolution and evaporation of the solvent prior to measurement allows for low-concentration photodecomposition studies, where similar detailed vibrations as the solid compound are obtained (**C1′** vs **C1**). Subtle inter- and intramolecular changes can result in noticeable shifts of the pyridine vibrational bands, while the azido and hydroxido stretches allow for the monitoring of the release and/or stability in the mid-IR region. The SR-FIR and Raman spectra show several strong and sharp platinum-ligand vibrations in the far-IR region, most notably the asymmetric and symmetric platinum−oxygen (OH) at 541/540 cm^{-1} (IR_{asym}/$Raman_{sym}$) and platinum−nitrogen (N_3) vibrations at 413/415 cm^{-1} (IR_{asym}/$Raman_{sym}$). Interestingly, the very strong Raman intensity of the Pt−N(N_3) vibration, υ_{sym}(N_3−Pt−N_3), proved to be related to the octahedral geometry of **C1**; thus, changes in the geometry of **C1** upon irradiation might be directly reflected in a reduction in the intensity of this vibration. Furthermore, photoinduced binding of **C1** to biomolecular targets can result in new platinum−ligand vibrations in the far-IR region. This is where the high sensitivity and strong group splitting of these platinum complexes by SR-FIR provides an invaluable window to study metal−ligand vibrations in detail.

CONCLUSIONS

Individual ligand (pyridine, hydroxido, and azido) and Pt-ligand vibrations for *trans,trans,trans*-[$Pt(N_3)_2(OH)_2(py)_2$] (**C1**), a photoactivatable diazido Pt(IV) anticancer prodrug candidate, have been obtained using ATR-FTIR, Raman, and SR-FIR spectroscopies and assigned by way of comparison with two of its synthetic precursors, *trans*-[$Pt(N_3)_2(py)_2$] (**C2**) and *trans*-[$PtCl_2(py)_2$] (**C3**). Synchrotron radiation allowed access to highly defined vibrational signatures in the far-IR range, which are otherwise challenging to obtain. Most notable of these were

DOI: 10.1021/acs.inorgchem.6b00476
Inorg. Chem. 2016, 55, 5983−5992

the strong Pt−OH vibrations (ca. 540 cm^{-1}) and the Pt−N_3 vibrations (415−395 cm^{-1}). These vibrations are also Raman-active, with the Raman spectrum also revealing multiple asymmetric azido stretching vibrations (2053−2018 cm^{-1}). DFT calculations were used to aid assignment of vibrational modes, with theoretical predictions found to be consistent with the experimental spectra. These vibrational data provide a basis for elucidating the dependence of photodecomposition and photoinduced biomolecular interactions of **C1** and related complexes on the nature of the ligand set in both the mid- and far-IR regions.

EXPERIMENTAL SECTION

Materials. All reactions were performed under nitrogen atmospheres using standard Schlenk techniques. K_2PtCl_4 (99%) was purchased from Precious Metals Online. All other chemicals and solvents were purchased from Sigma-Aldrich or BioScientific and used as received.

Synthesis. *trans*-[$PtCl_2(py)_2$] (**C3**) and *trans*-[$Pt(N_3)_2(py)_2$] (**C2**) were synthesized by published methods with characterization data in agreement with those reported previously.[10]

*trans,trans,trans-[$Pt(N_3)_2(OH)_2(py)_2$] (**C1**).* The synthesis was adapted from literature.[10] It was performed under strict exclusion of light, and purification was performed without prolonged exposure to light. *trans*-[$Pt(N_3)_2(py)_2$] (0.25 g, 0.57 mmol) was suspended in 30% H_2O_2 (20 mL) and stirred under nitrogen at 45 °C for 4 h resulting in a bright yellow solution. The solution was filtered while hot through a 0.2 μm polytetrafluoroethylene syringe filter and concentrated to 2 mL under reduced pressure. The crude compound was obtained by lyophilization and purified by column chromatography (silica, 40% methanol, 60% ethyl acetate) R_f = 0.5, to give **C1** > 95% pure by HPLC (87 mg, 32%). Characterization data were in agreement with those reported previously.[10]

Caution! *No problems were encountered during this work; however, heavy metal azides are known to be shock-sensitive detonators. Therefore, it is essential that excessive pressure is not applied to platinum azido compounds. Synthesis and all sample preparations were performed under strict exclusion of light.*

Instrumentation and Methods. *Thermal Evaporation.* A modified LBS500 sputter system was used for thermal evaporation. Plastic 96-well plates were coated with 100 nm silver by thermal evaporation to remove the Raman signals of the well plate and afford a reflective surface.

High-Performance Liquid Chromatography. An Agilent 1260 Infinity Analytical HPLC incorporated with an Infinity diode array detector (214/254 nm) was used with an Agilent Zorbax Eclipse Plus C-18 Rapid Resolution column (95 Å, 3.5 μm, 100 × 4.6 mm).

ATR-FTIR Measurements. Spectra were acquired on a Bruker model Equinox 55 FT-IR spectrometer fitted with a N_2-cooled mercury−cadmium−telluride detector. A Specac golden gate diamond or a Harrick silicon multiple reflection ATR accessory was used for spectral acquisition. The silicon ATR accessory was used to acquire spectra of samples in solvated state. For this purpose, 3 μL water solutions of **C1** (2 mM) were deposited on the silicon ATR followed by evaporation under a gentle N_2 flow resulting in a thin film of compound for direct measurement. The spectra were acquired with OPUS software 6.0. ATR spectra were collected in the wavenumber range between 4000 and 400 cm^{-1} at a spectral resolution of 4 cm^{-1}, and 50 interferograms were coadded.

Raman Measurements. Raman spectra were acquired on a Renishaw inVia instrument equipped with a Peltier-cooled CCD detector using a modified Leica DM LM optical microscope and a 633 nm Coherent HeNe laser. Two optical microscope objectives were used for spectral acquisition: an Olympus ULWD MS Plan 50*x*/0.55 for 96-well plate measurements and an Olympus SLMS Plans N 50*x*/0.35 for solid samples. Solid samples were measured on standard microscopy slides, and liquid samples (3−20 μL, 50 μM in Mili-Q water) were deposited in a silver-coated 96-well plate followed by evaporation under a gentle N_2 flow before measurement. The instrument was operated with WiRE software, calibrated against a silicon wafer. Single scan Raman spectra were collected in the wavenumber range between 4000 and 0 cm^{-1} with an exposure time of 10 s. The laser power on the samples was kept at ∼1 mW with a spectral resolution of ∼1 cm^{-1}.

SR-FIR Measurements. SR-FIR spectra were measured at the Terahertz/Far-IR beamline at the Australian Synchrotron (light source: 200 mA in top-up mode). Synchrotron radiation (SR) is an intrinsically bright source and is 100−1000 times brighter than commercial thermal (i.e., blackbody or globar) infrared sources.[68] While SR is no more powerful than a globar source, its effective source size is smaller, allowing for small beam-size measurements with high signal-to-noise ratios, which in turn can offer significant advantages for studies of small samples in the THz/far-IR region.[69]

Spectra were acquired on an IFS 125/HR Bruker FT spectrometer equipped with a 6 μm multilayer Mylar beamsplitter, a Si Bolometer detector, and an automated cryostat sample holder (ST-100, Janis Research), which holds three samples. Small samples (0.5−1.5 mg) were evenly spread on a 3 mm paraffin wax disk and pressed into the paraffin by applying delicate hand pressure using a 3 mm die set (Figure 8B). The 3 mm paraffin wax disks were prepared by pressing

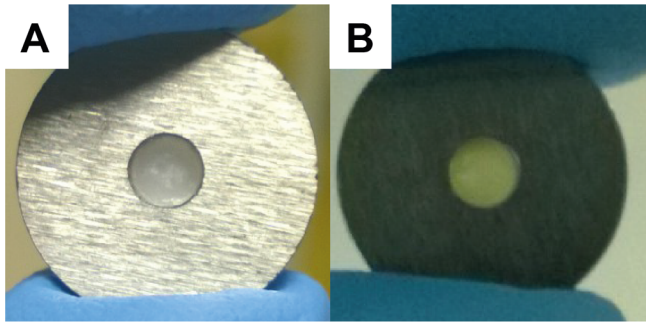

Figure 8. SR-FIR sample holders; (A) paraffin blank; (B) paraffin holding **C1** (1 mg).

roughly 20 mg of paraffin wax (Surgipath Paraplast, Leica Biosystems) in a 7 mm die set using a hand press (PIKE Technologies, pressure setting 6) followed by transferring the paraffin into a 3 mm die collar (Figure 8A). Transmission spectra were collected between 700 and 0 cm^{-1} at a spectral resolution of 1 cm^{-1} using a 3.15 mm aperture and 64 interferograms coadded at room temperature (ca. 301 K) and 77 K. Following this, a second measurement at room temperature was taken, and no discernible differences between the room-temperature spectra were observed.

Data Processing. Preprocessing of the spectral data was performed in OPUS software 7.2 (Bruker Optics). SR-FIR spectra were averaged (eight for **C1** and four for **C2** and **C3**) and transformed to absorbance prior to concave rubber-band baseline correction and vector normalization. Diamond ATR-FTIR spectra of solid/crystalline **C1**, **C2**, and **C3** exhibited anomalous dispersion (rapid changes to the refractive index of a sample while scanning through an absorption peak) resulting in asymmetric line shapes and shifts in absorption maxima[67] (Figure S14A). These artifacts were identical within replicates, and six spectra were first averaged followed by extended ATR correction to correct for these artifacts prior to concave rubber-band baseline correction and vector normalization. A detailed description of the extended ATR correction is given in the Supporting Information. Diamond and silicon ATR-FTIR spectra of **C1′** did not exhibit these artifacts (Figure S13), and averaged spectra (six) were only baseline-corrected (concave rubber-band) and vector-normalized. Only vector-normalization was applied to Raman spectra after an average was taken of six spectra. Second derivatives were obtained using nine smoothing points.

Computational Details. DFT calculations were performed using the Gaussian09 package[70] with the Perdew−Burke−Ernzerhof exchange correlation functional and Minnesota 06 Functional (M06-2X). A mixed basis set is used where a cc-pVDZ basis set was used for carbon, hydrogen, nitrogen, and oxygen and the cc-pVDZ-PP basis set[44] with effective core potentials (ECP) for platinum. Geometry optimization of

DOI: 10.1021/acs.inorgchem.6b00476
Inorg. Chem. 2016, 55, 5983−5992

the ground-state (S_0) of **C1**, **C2**, and **C3** were performed using the conductor-like polarizable continuum model (CPCM) with water as solvent to better describe the electrostatic interactions between platinum and ligands.[71−73] Gas-phase calculations were performed for comparison. By allowing all parameters to relax, the calculations converged to optimized geometries corresponding to true energy minima, as revealed by the lack of imaginary values in the vibrational mode calculations. A full conformation screening was performed on **C1**, **C2**, and **C3** by systematically changing all the dihedral angles for the respective complexes until corresponding minima were attained. Ground-state optimization of **C1** resulted in four S_0 geometries with PBE and M06-2X exchange-correlation functionals, respectively. Ground-state optimization of **C2** resulted in seven S_0 geometries each with PBE and M06-2X. Likewise, one S_0 geometry with PBE and two with M06-2X were obtained for **C3**. Ground-state lowest energy geometries (S_0) computed by theoretical calculations using CPCM were compared to the previously reported crystal structures, and closest matches from both PBE and M06-2X were used to match experimental vibrational results. The calculated IR frequencies and intensities were exported from GaussView 5;[74] IR peak half-width at half height: 4 cm^{-1}, step size 1 and visualized using OPUS software 7.2.

■ ASSOCIATED CONTENT

Supporting Information

The Supporting Information is available free of charge on the ACS Publications website at DOI: 10.1021/acs.inorgchem.6b00476.

A description of planes of the octahedral complex **C1**. C_{2v} symmetry and vibrational modes of pyridine bound to platinum. X-ray structures and selected bond distances and angles for **C1**, **C2**, and **C3**. Raman and ATR-FTIR spectra of **C1**, **C1′**, **C2**, and **C3**. Individual SR-FIR and calculated spectra of **C1**, **C2**, and **C3** at room temperature and 77 K. Crystal packing of **C2**. ATR-FTIR spectra of **C1′** on a diamond and silicon ATR accessory. Extended ATR correction methodology and the processing schematic used to correct for anomalous dispersion by extended ATR correction. ATR-FTIR spectra of **C1**, **C2**, and **C3** before and after extended ATR correction. Tabulated ATR-FTIR, Raman, SR-FIR, and theoretical vibrational bands of **C1**, **C2**, and **C3**. Comments on scaling of vibrational frequencies, including selected bond distances and asymmetric stretching vibrations of **C1**, **C2**, and **C3**. Cartesian coordinates of ground-state geometries of **C1**, **C2**, and **C3**. Calculated IR frequencies and intensities for **C1**, **C2**, and **C3** (unscaled). (PDF)

Data created during this research are openly available from the University of Warwick Research Archive Portal at http://wrap.warwick.ac.uk.

■ AUTHOR INFORMATION

Corresponding Authors

*E-mail: bayden.wood@monash.edu. (B.R.W.)
*E-mail: leone.spiccia@monash.edu. (L.S.)

Author Contributions

The manuscript was written through contributions of all authors. All authors have given approval to the final version of the manuscript.

Notes

The authors declare no competing financial interest.

■ ACKNOWLEDGMENTS

Financial support from the Australian Research Council in the form of Future Fellowship grants to B.R.W. (FT120100926) and B.G. (FT130100838) and a Discovery Outstanding Research Award (DORA) and Discovery Project to L.S. (DP130100816) is gratefully acknowledged. P.J.S. thanks the ERC (Grant No. 247450), EPSRC (Grant No. EP/F042159/1 and MOAC studentship for E.S.), and Science City (AWM/ERDF) for support. R.R.V. thanks the Monash Warwick Alliance for their support and travel funding as part of the Monash Univ. and the Univ. of Warwick Joint Ph.D. program. M.K. was supported by a Marie Curie International Outgoing Fellowship from the European Union's Seventh Framework Programme for research, technological development, and demonstration under Grant Agreement No. 627113. We acknowledge Mr. F. Shanks for instrumental support at the Centre for Biospectroscopy, Monash Univ. Synchrotron beam time to access the THz/Far-IR beamline was awarded by the Australian Synchrotron under the merit-based proposal scheme. We also acknowledge the Monash Campus HPC Cluster at the Monash eResearch Centre and eSolutions-Research Support Services for computational facilities.

■ REFERENCES

(1) Rosenberg, B.; Vancamp, L.; Trosko, J. E.; Mansour, V. H. *Nature* **1969**, *222*, 385−386.
(2) Kelland, L. *Nat. Rev. Cancer* **2007**, *7*, 573−584.
(3) Bernhard, L. *Cisplatin: Chemistry and biochemistry of a leading anticancer drug;* Verlag Helvetica Chimica Acta: Zurich, 1999.
(4) Dyson, P. J.; Sava, G. *Dalton Trans.* **2006**, 1929−1933.
(5) Rabik, C. A.; Dolan, M. E. *Cancer Treat. Rev.* **2007**, *33*, 9−23.
(6) Wang, D.; Lippard, S. J. *Nat. Rev. Drug Discovery* **2005**, *4*, 307−320 and references therein..
(7) Siddik, Z. H. *Oncogene* **2003**, *22*, 7265−7279.
(8) Wang, X.; Wang, X.; Guo, Z. *Acc. Chem. Res.* **2015**, *48*, 2622−2631.
(9) Johnstone, T. C.; Suntharalingam, K.; Lippard, S. J. *Chem. Rev.* **2016**, *36*, 1249−1262.
(10) Farrer, N. J.; Woods, J. A.; Salassa, L.; Zhao, Y.; Robinson, K. S.; Clarkson, G.; Mackay, F. S.; Sadler, P. J. *Angew. Chem., Int. Ed.* **2010**, *49*, 8905−8908.
(11) Butler, J. S.; Woods, J. A.; Farrer, N. J.; Newton, M. E.; Sadler, P. J. *J. Am. Chem. Soc.* **2012**, *134*, 16508−16511.
(12) Chin, C. F.; Tian, Q.; Setyawati, M. I.; Fang, W.; Tan, E. S. Q.; Leong, D. T.; Ang, W. H. *J. Med. Chem.* **2012**, *55*, 7571−7582.
(13) Zhao, Y.; Farrer, N. J.; Li, H.; Butler, J. S.; McQuitty, R. J.; Habtemariam, A.; Wang, F.; Sadler, P. J. *Angew. Chem., Int. Ed.* **2013**, *52*, 13633−13637.
(14) Zhao, Y.; Woods, J. A.; Farrer, N. J.; Robinson, K. S.; Pracharova, J.; Kasparkova, J.; Novakova, O.; Li, H.; Salassa, L.; Pizarro, A. M.; Clarkson, G. J.; Song, L.; Brabec, V.; Sadler, P. J. *Chem. - Eur. J.* **2013**, *19*, 9578−9591.
(15) Gandioso, A.; Shaili, E.; Massaguer, A.; Artigas, G.; Gonzalez-Canto, A.; Woods, J. A.; Sadler, P. J.; Marchan, V. *Chem. Commun.* **2015**, *51*, 9169−9172.
(16) Yuan, Y.; Kwok, R. T. K.; Tang, B. Z.; Liu, B. *J. Am. Chem. Soc.* **2014**, *136*, 2546−2554.
(17) Zheng, Y.-R.; Suntharalingam, K.; Johnstone, T. C.; Yoo, H.; Lin, W.; Brooks, J. G.; Lippard, S. J. *J. Am. Chem. Soc.* **2014**, *136*, 8790−8798.
(18) Zheng, Y.-R.; Suntharalingam, K.; Johnstone, T. C.; Lippard, S. J. *Chem. Sci.* **2015**, *6*, 1189−1193.
(19) Suntharalingam, K.; Song, Y.; Lippard, S. J. *Chem. Commun.* **2014**, *50*, 2465−2468.
(20) Harris, A. L. *Nat. Rev. Cancer* **2002**, *2*, 38−47.
(21) Mari, C.; Pierroz, V.; Ferrari, S.; Gasser, G. *Chem. Sci.* **2015**, *6*, 2660−2686 and references therein..
(22) Mari, C.; Pierroz, V.; Leonidova, A.; Ferrari, S.; Gasser, G. *Eur. J. Inorg. Chem.* **2015**, *2015*, 3879−3891.
(23) Knoll, J. D.; Turro, C. *Coord. Chem. Rev.* **2015**, *282*−*283*, 110−126 and references therein..

DOI: 10.1021/acs.inorgchem.6b00476
Inorg. Chem. 2016, 55, 5983−5992

(24) Farrer, N. J.; Salassa, L.; Sadler, P. J. *Dalton Trans.* **2009**, 10690−10701 and references therein..
(25) Wachter, E.; Heidary, D. K.; Howerton, B. S.; Parkin, S.; Glazer, E. C. *Chem. Commun.* **2012**, *48*, 9649−9651.
(26) Sgambellone, M. A.; David, A.; Garner, R. N.; Dunbar, K. R.; Turro, C. *J. Am. Chem. Soc.* **2013**, *135*, 11274−11282.
(27) Howerton, B. S.; Heidary, D. K.; Glazer, E. C. *J. Am. Chem. Soc.* **2012**, *134*, 8324−8327.
(28) Schatzschneider, U. *Eur. J. Inorg. Chem.* **2010**, *2010*, 1451−1467 and references therein.
(29) Bednarski, P. J.; Mackay, F. S.; Sadler, P. J. *Anti-Cancer Agents Med. Chem.* **2007**, *7*, 75−93 and references therein.
(30) Mackay, F. S.; Woods, J. A.; Heringova, P.; Kasparkova, J.; Pizarro, A. M.; Moggach, S. A.; Parsons, S.; Brabec, V.; Sadler, P. J. *Proc. Natl. Acad. Sci. U. S. A.* **2007**, *104*, 20743−20748.
(31) Pizarro, A. M.; McQuitty, R. J.; Mackay, F. S.; Zhao, Y.; Woods, J. A.; Sadler, P. J. *ChemMedChem* **2014**, *9*, 1169−1175.
(32) Pracharova, J.; Zerzankova, L.; Stepankova, J.; Novakova, O.; Farrer, N. J.; Sadler, P. J.; Brabec, V.; Kasparkova, J. *Chem. Res. Toxicol.* **2012**, *25*, 1099−1111.
(33) Baker, M. J.; Trevisan, J.; Bassan, P.; Bhargava, R.; Butler, H. J.; Dorling, K. M.; Fielden, P. R.; Fogarty, S. W.; Fullwood, N. J.; Heys, K. A.; Hughes, C.; Lasch, P.; Martin-Hirsch, P. L.; Obinaju, B.; Sockalingum, G. D.; Sulé-Suso, J.; Strong, R. J.; Walsh, M. J.; Wood, B. R.; Gardner, P.; Martin, F. L. *Nat. Protoc.* **2014**, *9*, 1771−1791.
(34) Meister, K.; Niesel, J.; Schatzschneider, U.; Metzler-Nolte, N.; Schmidt, D. A.; Havenith, M. *Angew. Chem., Int. Ed.* **2010**, *49*, 3310−3312.
(35) Quaroni, L.; Zobi, F., Cellular Imaging with Metal Carbonyl Complexes. In *Inorganic Chemical Biology;* John Wiley & Sons, Ltd: Chichester, U.K., 2014; pp 149−182.
(36) Kong, K. V.; Chew, W.; Lim, L. H. K.; Fan, W. Y.; Leong, W. K. *Bioconjugate Chem.* **2007**, *18*, 1370−1374.
(37) Jalkanen, K. J.; Würtz Jürgensen, V.; Claussen, A.; Rahim, A.; Jensen, G. M.; Wade, R. C.; Nardi, F.; Jung, C.; Degtyarenko, I. M.; Nieminen, R. M.; Herrmann, F.; Knapp-Mohammady, M.; Niehaus, T. A.; Frimand, K.; Suhai, S. *Int. J. Quantum Chem.* **2006**, *106*, 1160−1198.
(38) Berger, G.; Gasper, R.; Lamoral-Theys, D.; Wellner, A.; Gelbcke, M.; Gust, R.; Nève, J.; Kiss, R.; Goormaghtigh, E.; Dufrasne, F. *Int. J. Oncol.* **2010**, *37*, 679−686.
(39) Bambery, K. R.; Wood, B. R.; Schultke, E.; Juurlink, B. H. J.; May, T.; McNaughton, D., Monitoring the Effects of Cisplatin Uptake in Rat Glioma Cells: A Preliminary Study Using Fourier Transform Infrared Synchrotron Microspectroscopy. In *Biomedical Applications of Synchrotron Infrared Microspectroscopy: A Practical Approach;* The Royal Society of Chemistry: Cambridge, U.K., 2011; pp 339−350.
(40) Derenne, A.; Gasper, R.; Goormaghtigh, E. *Analyst* **2011**, *136*, 1134−1141.
(41) Mackay, F. S.; Farrer, N. J.; Salassa, L.; Tai, H.-C.; Deeth, R. J.; Moggach, S. A.; Wood, P. A.; Parsons, S.; Sadler, P. J. *Dalton Trans.* **2009**, 2315−2325.
(42) Johnstone, T. C.; Lippard, S. J. *J. Am. Chem. Soc.* **2014**, *136*, 2126−2134.
(43) Wilson, E. B. *Phys. Rev.* **1934**, *45*, 706−714.
(44) Figgen, D.; Peterson, K. A.; Dolg, M.; Stoll, H. *J. Chem. Phys.* **2009**, *130*, 164108.
(45) Kline, C. H.; Turkevich, J. *J. Chem. Phys.* **1944**, *12*, 300−309.
(46) Corrsin, L.; Fax, B. J.; Lord, R. C. *J. Chem. Phys.* **1953**, *21*, 1170−1176.
(47) Castellucci, E.; Sbrana, G.; Verderame, F. D. *J. Chem. Phys.* **1969**, *51*, 3762−3770.
(48) Dilella, D. P.; Stidham, H. D. *J. Raman Spectrosc.* **1980**, *9*, 90−106.
(49) Wong, K. N.; Colson, S. D. *J. Mol. Spectrosc.* **1984**, *104*, 129−151.
(50) Walters, V. A.; Snavely, D. L.; Colson, S. D.; Wiberg, K. B.; Wong, K. N. *J. Phys. Chem.* **1986**, *90*, 592−597.
(51) Wu, D.-Y.; Ren, B.; Jiang, Y.-X.; Xu, X.; Tian, Z.-Q. *J. Phys. Chem. A* **2002**, *106*, 9042−9052.
(52) Wu, D.-Y.; Duan, S.; Ren, B.; Tian, Z.-Q. *J. Raman Spectrosc.* **2005**, *36*, 533−540.
(53) Kumar, M.; Srivastava, M.; Yadav, R. A. *Spectrochim. Acta, Part A* **2013**, *111*, 242−251.
(54) Wu, D.-Y.; Hayashi, M.; Shiu, Y.-J.; Liang, K.-K.; Chang, C.-H.; Lin, S.-H. *J. Chin. Chem. Soc.* **2003**, *50*, 735−744.
(55) Ureña, F. P.; Gómez, M. F.; González, J. J. L.; Torres, E. M. n. *Spectrochim. Acta, Part A* **2003**, *59*, 2815−2839.
(56) Faggiani, R.; Howard-Lock, H. E.; Lock, C. J. L.; Lippert, B.; Rosenberg, B. *Can. J. Chem.* **1982**, *60*, 529−534.
(57) Guo, S.-X.; Mason, D. N.; Turland, S. A.; Lawrenz, E. T.; Kelly, L. C.; Fallon, G. D.; Gatehouse, B. M.; Bond, A. M.; Deacon, G. B.; Battle, A. R.; Hambley, T. W.; Rainone, S.; Webster, L. K.; Cullinane, C. *J. Inorg. Biochem.* **2012**, *115*, 226−239.
(58) Hambley, T. W.; Battle, A. R.; Deacon, G. B.; Lawrenz, E. T.; Fallon, G. D.; Gatehouse, B. M.; Webster, L. K.; Rainone, S. *J. Inorg. Biochem.* **1999**, *77*, 3−12.
(59) Johnstone, T.; Lippard, S. *JBIC, J. Biol. Inorg. Chem.* **2014**, *19*, 667−674.
(60) Wang, S.-L.; Johnston, C. T. *Am. Mineral.* **2000**, *85*, 739−744.
(61) Forster, D.; Horrocks, W. D. *Inorg. Chem.* **1966**, *5*, 1510−1514.
(62) Schmidtke, H.-H.; Garthoff, D. *J. Am. Chem. Soc.* **1967**, *89*, 1317−1321.
(63) Basile, L. Metal-Nitrogen Vibrations. In *Low-Frequency Vibrations of Inorganic and Coordination Compounds;* Springer Plenum Press: New York, 1971; pp 191−246.
(64) Adams, D. M.; Chatt, J.; Gerratt, J.; Westland, A. D. *J. Chem. Soc.* **1964**, *0*, 734−739.
(65) Clark, R. J. H.; Williams, C. S. *Inorg. Chem.* **1965**, *4*, 350−357.
(66) Ferraro, J. Metal Halide Vibrations. In *Low-Frequency Vibrations of Inorganic and Coordination Compounds;* Springer Plenum Press: New York, 1971; pp 111−189.
(67) Chalmers, J. M. Mid-Infrared Spectroscopy: Anomalies, Artifacts and Common Errors. In *Handbook of Vibrational Spectroscopy;* John Wiley & Sons, Ltd: 2006; pp 2327−2347.
(68) Duncan, W. D.; Williams, G. P. *Appl. Opt.* **1983**, *22*, 2914−2923.
(69) Brubach, J. B.; Manceron, L.; Rouzières, M.; Pirali, O.; Balcon, D.; Tchana, F. K.; Boudon, V.; Tudorie, M.; Huet, T.; Cuisset, A.; Roy, P. *AIP Conf. Proc.* **2009**, *1214*, 81−84.
(70) Frisch, M. J.; T, G. W.; Schlegel, H. B.; Scuseria, G. E.; Robb, M. A.; Cheeseman, J. R.; Scalmani, G.; Barone, V.; Mennucci, B.; Petersson, G. A.; Nakatsuji, H.; Caricato, M.; Li, X.; Hratchian, H. P.; Izmaylov, A. F.; Bloino, J.; Zheng, G.; Sonnenberg, J. L.; Hada, M.; Ehara, M.; Toyota, K.; Fukuda, R.; Hasegawa, J.; Ishida, M.; Nakajima, T.; Honda, Y.; Kitao, O.; Nakai, H.; Vreven, T.; Montgomery, J. A., Jr.; Peralta, J. E.; Ogliaro, F.; Bearpark, M.; Heyd, J. J.; Brothers, E.; Kudin, K. N.; Staroverov, V. N.; Kobayashi, R.; Normand, J.; Raghavachari, K.; Rendell, A.; Burant, J. C.; Iyengar, S. S.; Tomasi, J.; Cossi, M.; Rega, N.; Millam, M. J.; Klene, M.; Knox, J. E.; Cross, J. B.; Bakken, V.; Adamo, C.; Jaramillo, J.; Gomperts, R.; Stratmann, R. E.; Yazyev, O.; Austin, A. J.; Cammi, R.; Pomelli, C.; Ochterski, J. W.; Martin, R. L.; Morokuma, K.; Zakrzewski, V. G.; Voth, G. A.; Salvador, P.; Dannenberg, J. J.; Dapprich, S.; Daniels, A. D.; Farkas, Ö.; Foresman, J. B.; Ortiz, J. V.; Cioslowski, J.; Fox, D. J. *Gaussian 09,* Revision A.02; Gaussian, Inc: Wallingford, CT, 2009.
(71) Barone, V.; Cossi, M. *J. Phys. Chem. A* **1998**, *102*, 1995−2001.
(72) Cossi, M.; Rega, N.; Scalmani, G.; Barone, V. *J. Comput. Chem.* **2003**, *24*, 669−81.
(73) Tomasi, J.; Mennucci, B.; Cammi, R. *Chem. Rev.* **2005**, *105*, 2999−3094.
(74) Dennington, R.; Keith, T.; Millam, J. *GaussView,* Version 5; Semichem Inc: Shawnee Mission, KS, 2009.

DOI: 10.1021/acs.inorgchem.6b00476
Inorg. Chem. 2016, 55, 5983−5992